MULTICHANNEL AUTOFOCUS ALGORITHM FOR SYNTHETIC APERTURE RADAR

Robert L. Morrison, Jr. and Minh N. Do

Department of Electrical and Computer Engineering
Coordinated Science Laboratory
University of Illinois at Urbana-Champaign
rlmorris@uiuc.edu, minhdo@uiuc.edu

ABSTRACT

The autofocus problem in synthetic aperture radar (SAR) is considered, where phase errors in the acquired signal data result in imagery that is improperly focused. We present a new non-iterative approach to SAR autofocus, termed the MultiChannel Autofocus (MCA) algorithm, that allows the image focusing operator to be determined directly using a linear algebraic formulation. Specifically, we exploit the multichannel redundancy of the defocusing operation to create a linear subspace framework, where the unknown perfectly-focused image can be expressed in terms of a known basis expansion. By invoking an additional assumption on the underlying image support, the framework becomes sufficiently constrained so that a unique focusing filter can be solved for. The MCA approach is found to be computationally efficient and robust, and does not require prior assumptions about the characteristics of the SAR scene; the performance of previous SAR autofocus techniques relies upon the accuracy of priors such as sharpness metrics or dominant point scatterers. We present experimental results characterizing the performance of MCA in comparison with conventional autofocus methods, and discuss the practical implementation of the technique.

1. INTRODUCTION

SAR imaging systems are often subject to demodulation timing errors at the radar receiver that result from unknown delays in the received signals [1]. Such delays can be due to uncertainties in the radar platform position, or due to signal propagation through a medium with spatially-varying propagation velocity. The effect of the demodulation timing errors is to cause the Fourier transform of the SAR image to be corrupted with multiplicative phase errors. As a result, the produced SAR imagery is improperly focused.

Many approaches to *data-driven autofocus* have been proposed for SAR, where the goal is to restore the perfectly-focused image given the defocused image and assumptions about the SAR scene [2],[3]. In these approaches, the phase error is modeled as a 1-D function of the cross-range dimension in the Fourier domain, so that each column of the perfectly-focused image is defocused by a common blurring kernel. In our previous work [4], we identified this as the *multichannel condition* of SAR autofocus, and we showed that this provides an explicit basis expansion for the unknown perfectly focused image in terms of the defocused image. The success of existing SAR autofocus methods requires accurate prior assumptions about the underlying SAR scene, such as image sharpness metrics or the existence of point scatterers. Since these methods tend to perform poorly when the prior assumptions are not accurate, it is of interest to directly exploit the linear structure of the SAR autofocus problem arising from the multichannel condition.

In this paper, we present a new approach to SAR autofocus, termed the *MultiChannel Autofocus (MCA)* algorithm, where the image focusing operator is determined directly using a linear algebraic formulation. Specifically, we use the subspace characterization for the perfectly-focused image in [4] to create a linear framework through which we can solve for a correction filter (i.e., the inverse of the blurring kernel). We note that in our previous work, we used sharpness metric optimization to determine a unique solution within this subspace. However, in this work we utilize an *image support condition* instead that allows the correction filter to be obtained as the solution of a known linear system of equations. Specifically, we require a small portion of the perfectly-focused image to be zero-valued (or correspond to a region of low return). This constrains the problem sufficiently so that a unique correction filter can be solved for. Thus, the solution is determined in a non-iterative fashion, and does not require the use of priors such as image sharpness metrics. In practice, the desired image support condition can be achieved by exploiting the spatially-limited illumination of the antenna beam. In addition, inverse SAR (ISAR) images typically consist of man-made targets against a low-return background.

The MCA approach is found to be computationally efficient, and robust with respect to deviations from the ideal image support assumption. In addition, the technique accurately corrects all classes of phase errors; the performance of existing approaches sometimes suffers considerably when the phase errors are large and rapidly-varying.

2. SUBSPACE FRAMEWORK FOR SAR AUTOFOCUS

2.1. Complete Characterization of the Solution Space

We denote $\boldsymbol{g} \in \mathbb{C}^{M \times N}$ and $\tilde{\boldsymbol{g}} \in \mathbb{C}^{M \times N}$ to be the perfectly-focused and defocused SAR images, respectively, where the rows correspond to the cross-range coordinate and the columns to the range coordinate. The phase errors in SAR can be modeled by a 1-D phase error function $\phi_e[k_m]$ that applies a constant phase shift to each row of the Fourier-domain data [1]:

$$\tilde{G}[k_m, n] = G[k_m, n] e^{j\phi_e[k_m]} \tag{1}$$

where k_m is a discrete frequency index in the cross-range dimension, n is a discrete spatial-domain index in the range dimension, and $G[k_m, n] = DFT_m\{g[m, n]\}$.

Using matrix notation, the defocusing relationship in the spatial

This work was supported by the National Science Foundation under Grant CCR 0430877.

domain is expressed as:

$$\tilde{\boldsymbol{g}} = \underbrace{\boldsymbol{F}^H \boldsymbol{D}(e^{j\boldsymbol{\phi_e}})\boldsymbol{F}}_{\boldsymbol{C}\{\boldsymbol{b}\}} \boldsymbol{g} \tag{2}$$

where $\boldsymbol{F} \in \mathbb{C}^{M\times M}$ is the 1-D DFT operator with entries $F_{k_m,m} = \frac{1}{\sqrt{M}} e^{-j\frac{2\pi k_m m}{M}}$, $\boldsymbol{D}(e^{j\boldsymbol{\phi_e}}) \in \mathbb{C}^{M\times M}$ is a diagonal matrix with the entries $e^{j\phi_e[k_m]}$ on the diagonal, and $\boldsymbol{C}\{\boldsymbol{b}\} \in \mathbb{C}^{M\times M}$ is a circulant matrix formed with the blurring kernel $\boldsymbol{b}$, where $b[m] = DFT^{-1}_{k_m}\{e^{j\phi_e[k_m]}\}$. Thus, the defocusing effect can be described as the multiplication of the perfectly-focused image by a circulant matrix with eigenvalues equal to the unknown phase errors.

We define the *solution space* to be the set of all images formed from $\tilde{\boldsymbol{g}}$ with different $\hat{\phi}$:

$$\hat{\boldsymbol{g}} = \underbrace{\boldsymbol{F}^H \boldsymbol{D}(e^{j\hat{\phi}})\boldsymbol{F}}_{\boldsymbol{C}\{\boldsymbol{f_A}\}} \tilde{\boldsymbol{g}} \tag{3}$$

where $\boldsymbol{f_A}$ is an *all-pass* correction filter. The aim of SAR autofocus is to determine $\hat{\phi}$, or equivalently $\boldsymbol{f_A}$, so that $\hat{\boldsymbol{g}} = \boldsymbol{g}$ (i.e., $\hat{\phi} = -\phi_e$).

2.2. Explicit Multichannel Condition

To motivate the new MCA approach, we briefly review the subspace setup for the autofocus problem from [4]. Our goal is to create a *subspace* for the perfectly-focused image $\boldsymbol{g}$, spanned by a basis constructed from the defocused image $\tilde{\boldsymbol{g}}$. To accomplish this, we generalize the relationship in (3) to include *all* correction filters $\boldsymbol{f} \in \mathbb{C}^M$, that is, not just the subset of all-pass correction filters $\boldsymbol{f_A}$. As a result, we obtain an M-dimensional subspace where the perfectly-focused image $\boldsymbol{g}$ lives:

$$\hat{\boldsymbol{g}} = \boldsymbol{C}\{\boldsymbol{f}\}\tilde{\boldsymbol{g}}. \tag{4}$$

This subspace characterization explicitly captures the *multichannel condition* of SAR autofocus: the assumption that each column of the image is defocused by the same blurring kernel.

To produce a basis expansion for the subspace in terms of $\tilde{\boldsymbol{g}}$, we select any basis $\{\boldsymbol{e}_m\}_{m=0}^{M-1}$ for $\mathbb{C}^M$, and express the correction filter as:

$$\boldsymbol{f} = \sum_{m=0}^{M-1} f_m \, \boldsymbol{e}_m.$$

From this, any image $\hat{\boldsymbol{g}}$ in the subspace can be expressed in terms of a basis expansion as

$$\hat{\boldsymbol{g}} = \sum_{m=0}^{M-1} f_m \, \boldsymbol{\varphi}^{(m)}, \tag{5}$$

where

$$\boldsymbol{\varphi}^{(m)} = \boldsymbol{C}\{\boldsymbol{e}_m\}\tilde{\boldsymbol{g}} \tag{6}$$

are known basis vectors for the M-dimensional subspace containing the solution.

3. MCA DIRECT SOLUTION APPROACH

To formulate the MCA approach, we express the unknown perfectly-focused image in terms of the basis expansion in (5):

$$\mathbf{vec}\{\boldsymbol{g}\} = \boldsymbol{\Phi}\boldsymbol{f}, \tag{7}$$

where $\mathbf{vec}\{\boldsymbol{g}\}$ is an $MN \times 1$ vector composed of the concatenated columns of $\boldsymbol{g}$, and the columns of $\boldsymbol{\Phi}$ are the basis vectors $\mathbf{vec}\{\boldsymbol{\varphi}^{(m)}\}$ in (6). Here, the matrix $\boldsymbol{\Phi}$ is known, but $\boldsymbol{g}$ and $\boldsymbol{f}$ are unknown. By imposing an image support constraint on the perfectly-focused image $\boldsymbol{g}$, the linear system in (7) can be constrained sufficiently so that the unknown correction filter $\boldsymbol{f}$ can be directly solved for. Specifically, we assume that the $\boldsymbol{g}$ is non-zero only over a particular known region of support (ROS):

$$g[m,n] = \begin{cases} g'[m,n] & \text{for } m = 0,1,...,L-1 \\ 0 & \text{for } m = L, L+1, ..., M-1; \end{cases} \tag{8}$$

without loss of generality, we assume that the zero constraints appear as a contiguous block in the last $M - L$ rows.

Enforcing spatially-limited constraint directly into multichannel framework, (7) becomes:

$$\begin{bmatrix} \mathbf{0} \\ \mathbf{vec}\{\boldsymbol{g'}\} \end{bmatrix} = \begin{bmatrix} \boldsymbol{\Phi}_0 \\ \boldsymbol{\Phi'} \end{bmatrix} \boldsymbol{f} \tag{9}$$

where $\mathbf{0}$ is a vector of the zero constraints, $\boldsymbol{\Phi}_0$ are the rows of $\boldsymbol{\Phi}$ that correspond to the zero constraints, and $\boldsymbol{\Phi'}$ are the rows of $\boldsymbol{\Phi}$ that correspond to the unknown pixel values of $\boldsymbol{g}$ within the ROS. Given that $\mathbf{0}$ has dimension M or greater (i.e., there are at least M zero constraints), the correction filter $\boldsymbol{f}$ can be uniquely determined up to a scaling constant by solving

$$\boldsymbol{\Phi}_0 \boldsymbol{f} = \mathbf{0}. \tag{10}$$

We denote this direct linear solution method for determining the correction filter as the *MultiChannel Autofocus* (MCA) approach.

The approach assumes that $\boldsymbol{\Phi}_0$ is a rank $M-1$ matrix, which is satisfied when $\boldsymbol{g'}$ has full row rank; this is a consequence of $\boldsymbol{C}\{\boldsymbol{b}\}$ being square and invertible (except in degenerate cases), so that rank($\tilde{\boldsymbol{g}}$) = rank($\boldsymbol{g}$). The solution $\hat{\boldsymbol{f}}$ to (10) can be obtained by determining the unique nullvector of $\boldsymbol{\Phi}_0$:

$$\hat{\boldsymbol{f}} = \text{Null}(\boldsymbol{\Phi}_0) = \alpha \boldsymbol{f}, \tag{11}$$

where α is an arbitrary complex constant. To eliminate the scaling ambiguity, we use the Fourier phase of $\hat{\boldsymbol{f}}$ to correct the defocused image according to (3):

$$\hat{\phi}[k_m] = \angle\Big(DFT_m\{\hat{f}[m]\}\Big).$$

In other words, the all-pass condition of $\hat{\boldsymbol{f}}$ is used to determine a unique solution from (11).

When the image support assumption is only approximate ($\boldsymbol{\Phi}_0\boldsymbol{f} \simeq 0$), $\boldsymbol{\Phi}_0$ has full rank. In this case, $\hat{\boldsymbol{f}}$ can be determined as the minimum right singular vector using the SVD. We note that it is not necessary to enforce every zero-valued constraint; it is sufficient to use only a subset of the constraints as long as $\boldsymbol{\Phi}_0$ retains rank $M-1$. We can always determine a set of M constraints so that a unique solution can be determined. Thus, the computational cost of MCA is dominated by the computation of the minimum singular vector of the M by M matrix $\boldsymbol{\Phi}_0$. However, when the image support condition is only approximate, then the solution may be improved by using a number of constraints greater than M.

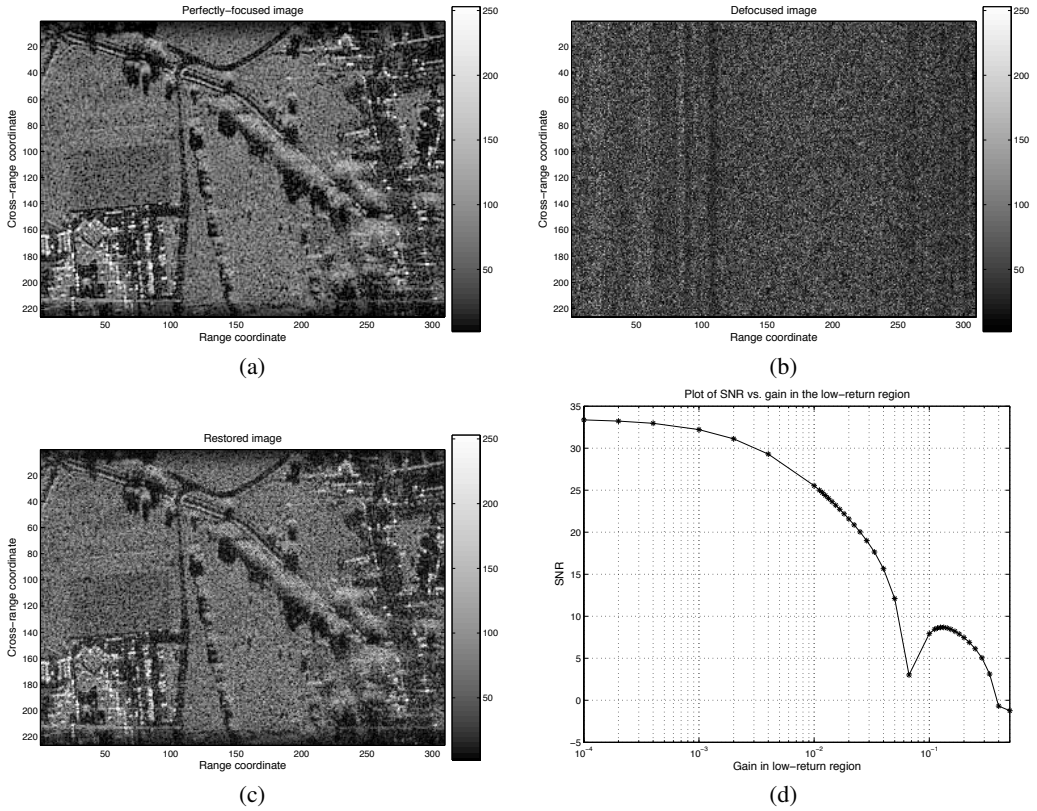

Fig. 1. Simulated 226 by 309 pixel SAR image: (a) perfectly-focused image, where a window function has been applied to each column of the SAR scene to simulate the antenna footprint (the window gain in the low-return region is 0.2), (b) defocused image produced by applying a white phase error function, (c) restoration formed using the MCA approach (SNR = 7.46, run time: 2.45 s), and (d) plot of the SNR of the MCA restoration vs. the window gain in the low-return region.

4. PRACTICAL IMPLEMENTATION

The area of terrain that can be imaged in SAR depends on the *antenna footprint*, which is the portion of the scene that is illuminated as determined by the projection of the antenna beam onto the ground plane. There is low return from features outside of the antenna footprint. The fact the SAR image is intrinsically spatially-limited, due to the finite range of illumination provided by the antenna, suggests that the proposed autofocus technique can be applied in general SAR imaging scenarios given that the SAR data are acquired properly. Specifically, the Fourier domain sampling density can be selected such that the field of view (FOV) of the SAR image extends beyond the illuminated portion of the scene in the cross-range dimension. In practice, the desired cross-range Fourier sampling density can be achieved by properly selecting the radar pulse repetition rate [1].

5. EXPERIMENTAL RESULTS

Figure 1 presents an experiment where we simulate the effect of the antenna footprint by applying a spatial-domain window to each column of a synthesized SAR scene. A SAR image from Sandia Laboratory is used as a model for the magnitude of the SAR scene, while the phase of each pixel in the spatial domain is selected at random (uniformly distributed between $-\pi$ and π and uncorrelated). The applied window function has unity gain over most of the image, and drops off towards the top and bottom of the image, attenuating the first and last set of rows. In the perfectly-focused image of Figure 1(a), the top and bottom rows are attenuated by a factor of 5, so that there are small, but non-negligible pixel magnitudes in these regions. A defocused version of the image, formed by applying a white Fourier phase error (i.e., independent phase components uniformly distributed between $-\pi$ and π) is shown in Figure 1(b); the white phase error is considered as a worst-case scenario, producing the most severe defocusing effects. The MCA restoration, assuming the top and bottom rows of the underlying image to be identically zero, is displayed in Figure 1(c). The restoration result indicates that MCA is robust to deviations from the ideal zero-return assumption.

To quantify the robustness of MCA with respect to the signal level in the low-return region, we varied the gain of the window function at the edges of the image, and determined the SNR of the resulting MCA restoration (the SNR is defined with respect to the perfectly-focused image). Figure 1(d) shows a plot of the SNR versus the gain in the low return region. The SNR is observed to decrease monotonically as the gain increases to 0.067, and then to increase and decrease again. For window gain values greater than 0.067, the restorations are incorrectly cyclicly shifted along each column by one pixel, but otherwise accurately resemble the perfectly-focused image, as is the case with the restoration in Figure 1(c) where the gain factor is 0.2. We observe that for SNR values less than 3 dB, the restored images do not resemble the perfectly-focused

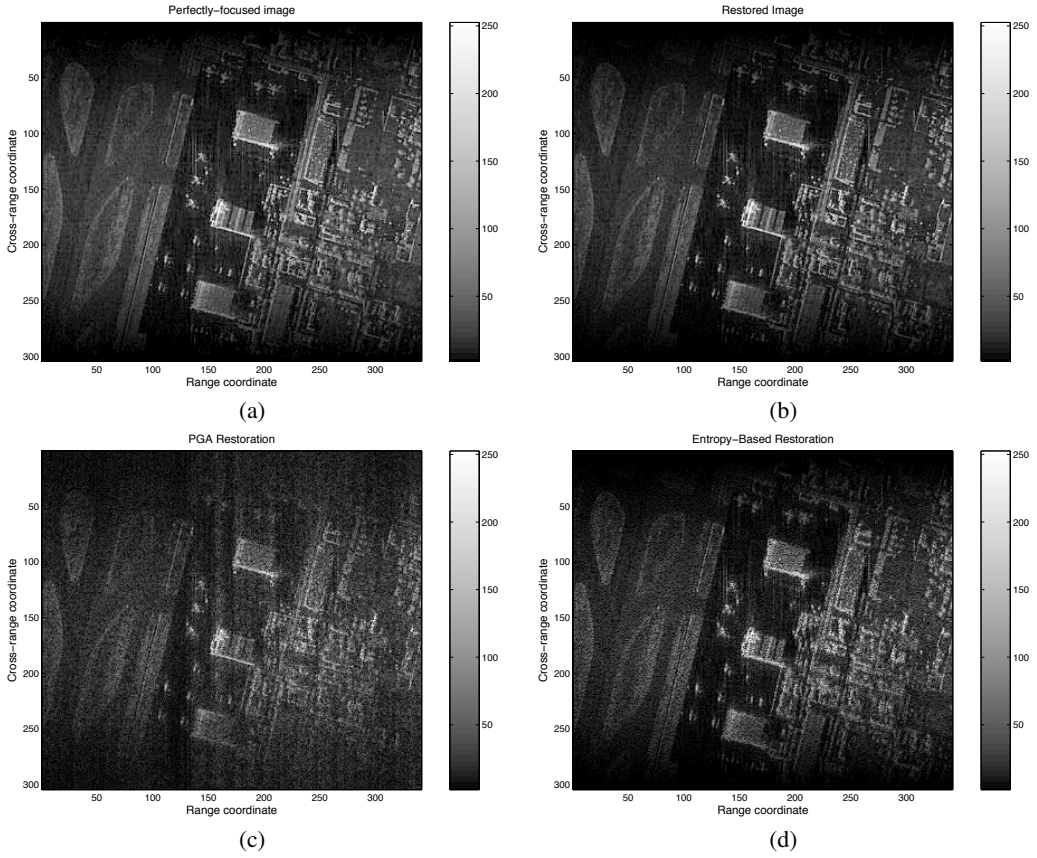

Fig. 2. Comparison of MCA with existing autofocus techniques: (a) 304 by 341 pixel perfectly-focused image, where a Hamming-weighted sinc window has been applied to each column of the synthesized SAR scene, (b) restored image using MCA (SNR $= 21.96$, run time: 3.97 s) , (c) PGA restoration (SNR $= 4.5561$, run time: 5.41 s), and (d) restoration using an entropy-based autofocus technique (SNR $= 2.90$, run time: 66.77 s).

image.

Figure 2 presents a realistic simulation of a SAR imaging experiment, where a Hamming-weighted sinc window, representative of an actual ground plane antenna pattern, has been applied to each column of the synthesized SAR scene. The perfectly-focused image in Figure 2(a) is formed from computed samples of the Fourier transform, where the sample spacing is selected so that the image FOV falls within a few pixels of the main lobe of the sinc window; in this case, there is some spatial-domain aliasing resulting from signal outside the FOV. To compare the performance of MCA with conventional autofocus techniques, we formed a defocused image using a white phase error function. The restoration result using MCA, assuming the top two and bottom two rows of the perfectly-focused image to be identically zero, is displayed in Figure 2(b). The MCA restoration is observed to agree well with the perfectly-focused image, having SNR $= 21.96$. A restoration using Phase Gradient Autofocus (PGA)[2] is shown in Figure 2(c) (SNR $= 4.5561$), while a restoration using a gradient-based entropy minimization autofocus technique [3] is displayed in Figure 2(d) (SNR $= 2.90$). Of the three autofocus approaches, MCA is found to produce the highest quality restoration in terms of qualitative comparison and SNR; it should be noted that while the entropy-based restoration more closely resembles the perfectly-focused image than the PGA restoration, it has a lower SNR because the entropy technique incorrectly accentuates some of the point scatterers. The computation times of MCA, PGA, and the entropy-based method were 3.97 s, 5.41 s, and 66.77 s, respectively.

6. REFERENCES

[1] C. V. Jakowatz, Jr., D. E. Wahl, P. H. Eichel, D. C. Ghiglia, and P. A. Thompson, *Spotlight-Mode Synthetic Aperture Radar: A Signal Processing Approach.*, Kluwer Academic Publishers, Boston, 1996.

[2] C. V. Jakowatz, Jr. and D. E. Wahl, "Eigenvector method for maximum-likelihood estimation of phase errors in synthetic-aperture-radar imagery," *J. Opt. Soc. Am. A*, vol. 10, no. 12, pp. 2539–2546, December 1993.

[3] J.R. Fienup and J. J. Miller, "Aberration correction by maximizing generalized sharpness metrics," *Journal of the Optical Society of America A*, vol. 20, no. 4, pp. 609–620, April 2003.

[4] R. L. Morrison, Jr. and M. N. Do, "A multichannel approach to metric-based SAR autofocus," in *Proc. of the IEEE International Conference on Image Processing*, Genoa, Italy, 2005, vol. 2, pp. 1070–1073.